Contactless Power Transfer – Theoretical Principles and Fields of Applications

Andrei Marinescu*, Mihai Iordache[†] and Lucian Mandache[◊]

* R&D Institute ICMET, Craiova, Romania, amarin@icmet.ro
† Faculty of Electrical Engineering, University Politehnica of Bucharest, Bucharest, Romania, mihai.iordache@upb.ro
◊ Faculty of Electrical Engineering, University of Craiova, Romania, lmandache@elth.ucv.ro

Abstract - **Contactless energy transfer [1] has indubitable advantages in modern technique given by the lack of electro-mechanical contacts predisposed to pitting and failure: use in aggressive or explosive (no sparks) environments, application to mechanisms with translation or rotation move-ments (robotics), high efficiency on relatively short distances a.s.o. Recent researches carried out in Romania demonstrate the feasibility of these systems for a wide power range, from a few watts up to tens of kW, suitable for the expansion of the electro-mobility and proliferation of multimedia and mobile communication devices. Such systems impose storing the energy in batteries requiring frequent charging. The concept of high frequency transformer with separable windings, as well as a capacitor with separable electrodes working in near field regime, the use of resonance and magnetic flux concentrators for increasing the transfer efficiency, some practical achievements and also maintaining of electromagnetic compatibility within well-defined limits are presented. The paper aims to draw the attention of users and also of prospective investors on the applications and advantages of these systems and to encourage national partnerships for developing theoretical and applied research in this field.**

Cuvinte cheie: *Transfer de energie fără contact; câmp apropiat; cuplaj inductiv; cuplaj capacitiv; aplicații.*

Keywords: *Contactless energy transfer; near field; inductive coupling; capacitive coupling; applications.*

I. INTRODUCTION

The subject of contactless energy transfer gained an increasing interest of scientific community, in order to exploit its indubitable benefits. The first application of power transfer in the near field was developed by Nikola Tesla who invented the induction motor where energy is transmitted from the fixed coil to the rotor across the air gap (1893). He envisaged developing a "global system for wireless energy transmission" providing free energy for all citizens. This infeasible idea was not agreed by investors, and the required funds were not granted.

The reference moment in modern history for contactless energy transmission was in 1980, when John Boys and collaborators from the University in Auckland exploited the principle of inductive power transfer in conveyers used in the industry. In 1991, A. Esser and H. Scudelny from the University of Aachen achieved the first wireless transmission for objects in motion.

Contactless energy transfer is not yet a well-recognized technique with reliable solutions, design methods and practical application experience. Most publications consider the theoretical aspects while the practical ones are not supported by product standards that allow the development of compatible equipment [1-6].

The strongest stimulus for achievements in this field is provided by electro-mobility and mobile phones migrating to smartphones with their important energy demand. In terms of the level of transmitted power, contactless charging of batteries in electric or hybrid vehicles is a key challenge.

Theoretical achievements are reported in Europe, with no considerable practical implementation. By contrast, South-East Asia and the US prove a higher interest for this technology [2,3]. Market analyses indicate that global wireless charger market will expand to $ 4.6 billion by 2019 [7].

Contactless power transfer is possible for short and medium distances through near field techniques (by capacitive coupling or inductive coupling), as well as long distances, through far field techniques (such as solar energy transmission through conversion to microwaves).

This paper presents the theoretical principles of near field energy transmission, as well as some applications, aiming to draw attention of users and prospective investors to the benefits and possibilities for implementation of these systems in current practice. Fig. 1 shows the schematic diagram for the two techniques of near field energy transmission, through capacitive coupling (a) and inductive coupling respectively (b), the two techniques being dual systems [6].

The study is based on the Maxwell-Hertz theory and it is focused on solutions for maximizing the energy transfer efficiency, which is essential for practical applications. The theoretical study is accompanied by numerical analyses and experimental results.
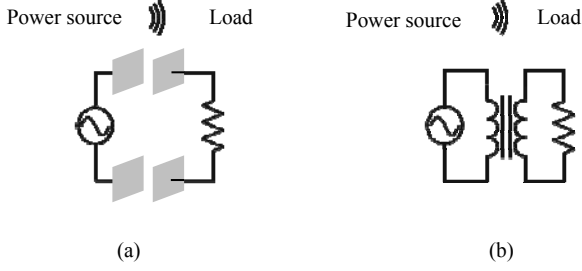

Fig. 1. Contactless power transfer systems, in near field:
(a) – capacitive transfer; (b) – inductive transfer.

II. PRINCIPLE OF ENERGY TRANSMISSION THROUGH CAPACITIVE COUPLING

The capacitive transfer shown as principle in Figure 1a is carried by the electric field (displacement current), an example being shown in Figure 2 [2], where the load resistance R (the load is assumed as purely resistive), is connected to the power supply through a capacitive coupling with two identical sections of capacitance C. A matching impedance (R_a, L_a) interlaced between the power source of voltage v_0 and the capacitive coupling provides the conditions for maximum transfer of power to the load. The resistance R_a includes both the resistance of the inductor L_a and the internal resistance of the power source.
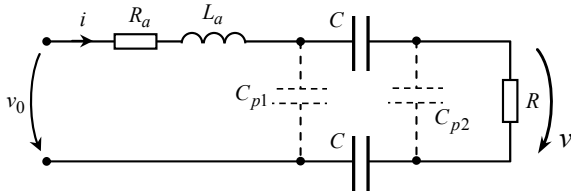

Fig. 2. Equivalent diagram of capacitive coupling transfer system.

A capacitive coupling system with planar capacitors will be considered (Fig. 1a), neglecting the parasitic capacitance on the source side, and on the load side respectively, shown in Figure 2. The electric field parameters in the capacitive coupling are detailed in Figure 3a, where a closed surface Σ (with the surface element $\overline{ds}$) has been chosen to allow the calculation of the electric flux density based on the law of electric flux. The segment AB (with the length element $\overline{dl}$) drawn between the armatures allows computing the voltage as line integral of electric field strength. With the armatures of surface S and the gap between them of length g, by assuming the spatial distribution of the electric field with plane-parallel symmetry, the local state quantities of the electric field are expressed in terms of a random value of the electric charge on the ar-mature q:

$$D = \frac{q}{S}; \quad E = \frac{q}{\varepsilon_0 S} = \frac{v_C}{g} \ . \tag{1}$$

The density of the displacement current:

$$J_d = \frac{dD}{dt} = \frac{1}{S}\frac{dq}{dt} = \frac{\varepsilon_0}{g}\frac{dv_C}{dt} , \tag{2}$$

leads to the displacement current which is equal to the conduction current through the terminals (according to the law of charge conservation):

$$i_d = S J_d = \frac{\varepsilon_0 S}{g}\frac{dv_C}{dt} = C\frac{dv_C}{dt} , \tag{3}$$

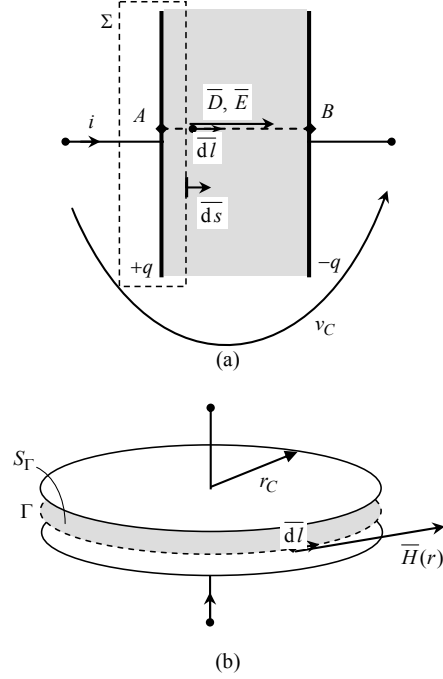where the capacitance C of the structure occurs.

Fig. 3. Explanatory diagram for the calculation of electric field parameters (a) and magnetic field parameters (b) for near field capacitive coupling.

To calculate the power transferred to the load, a sinusoidal supply voltage is considered:

$$v_0(t) = \sqrt{2}V_0 \sin(\omega t) , \text{ with the complex form } \underline{V}_0 = V_0. \tag{4}$$

The impedance of the circuit viewed by source terminals, the load current and voltage across the load resistance are:

$$\underline{Z} = R_a + R + j\left(\omega L_a - \frac{2}{\omega C}\right); \tag{5}$$

$$\underline{I} = \frac{1}{R_a + R + j\left(\omega L_a - \dfrac{2}{\omega C}\right)} \cdot V_0 \tag{6}$$

$$\underline{V} = \frac{R}{R_a + R + j\left(\omega L_a - \dfrac{2}{\omega C}\right)} \cdot V_0 . \tag{7}$$

The active power on the load and its peak value achieved in resonance conditions at a working frequency of $f_0 = 1/\pi\sqrt{2L_a C}$ are:

$$P = \text{Re}\left(\underline{V} \cdot \underline{I}^*\right) = \frac{R}{(R_a + R)^2 + \left(\omega L_a - \dfrac{2}{\omega C}\right)^2} \cdot V_0^2, \quad (8)$$

$$P_{max} = \frac{R}{(R_a + R)^2} \cdot V_0^2. \quad (9)$$

The active power supplied by the source:

$$P_0 = \text{Re}\left(\underline{V}_0 \underline{I}^*\right) = \frac{R_a + R}{(R_a + R)^2 + \left(\omega L_a - \dfrac{2}{\omega C}\right)^2} \cdot V_0^2. \quad (10)$$

leads to the transfer efficiency

$$\eta = \frac{P}{P_0} = \frac{1}{1 + \dfrac{R_a}{R}}. \quad (11)$$

The efficiency may be increased by decreasing the matching resistance R_a, which also leads to an increase of the circuit quality factor:

$$Q = \frac{1}{R_a + R}\sqrt{\frac{2L}{C}}. \quad (12)$$

As an image of system behavior, Figure 4 shows the power transferred to the load as a function of frequency for three different values of R_a; the quality factors and efficiencies are also shown. Planar armatures were considered for numerical applications, with a gap of 250mm; these values can be achieved in the case of electric buses with contactless battery charging systems.
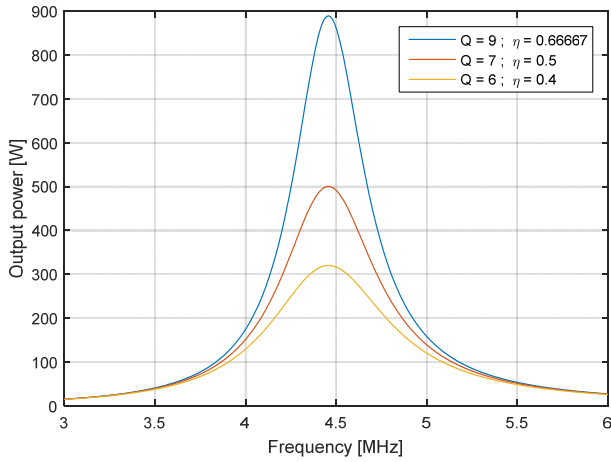

Fig. 4. Power transferred to the load for different values of matching resistance R_a.

This structure leads to $C = 255\,\text{pF}$ and, if $L_a = 10\,\mu\text{H}$ is chosen, the resonance frequency $f_0 = 4.45\,\text{MHz}$ is obtained. With $V_0 = 200\,\text{V}$, $R = 20\,\Omega$, it results that $Q = 6$ and $\eta = 0.4$. The peak value of the capacitor voltage is $V_{C\,max} = I_{max}/2\pi f_0 C = 560\,\text{V}$, with a corresponding peak value of the electric field strength of $\hat{E}_{max} = \sqrt{2}V_{C\,max}/g = 3.2\,\text{kV/m}$. The peak value of the power transferred to the load in these conditions is $P_{max} = 320\,\text{W}$ at the RMS value of the current of $I_{max} = 4\,\text{A}$. A deviation of the working frequency of 5 % against f_0 leads to a reduction of output power of about 25%.

It should be noticed that the size of the system is about one order of magnitude smaller than the wavelength corresponding to the resonance frequency ($\lambda = 67$ m), and the magnetic field in the dielectric is negligible.

In order to assess the magnetic field quantities, a disk-shaped capacitor is chosen (Fig. 3b), with the same capacitance as the previously considered one, the same gap length between armatures, the same dielectric material (air), and operating in the same conditions. The magnetic field strength in the dielectric will be computed on a circle of radius r (shown as the closed curve Γ in Fig. 3b), using the law of magnetic circuit expressed on the circle Γ which bounds the disk surface $S\Gamma$. For the periphery of the capacitor ($r = r_c = 1.4$ m) the magnetomotive force on Γ is equal to the total displacement current given by (3): $\displaystyle\int_{\Gamma} \overline{H} \cdot \text{d}\overline{l} = i_d$, which leads to the peak value of H in resonance conditions: $\hat{H}_{max} = \sqrt{2}I_{max}/2\pi r_C = 0.65\,\text{A/m}$ and the corresponding flux density $\hat{B}_{max} = 0.8\,\mu\text{T}$.

III. PRINCIPLE OF ENERGY TRANSMISSION THROUGH INDUCTIVE COUPLING

The inductive power transfer occurs by means of the magnetic field, as in the voltage or current transformers. However, for typical contactless power transfer applications, open magnetic core or coreless units are more suitable. The operating principle of such a system is explained for a transmitter coil with N_1 turns and a receiver coil with N_2 turns. Both are assumed as solenoidal coils disposed coaxially as in Figure 5a, their lengths being noticeably greater than the diameters $(l_1 \gg D_1,\ l_2 \gg D_2)$. In this particular case, the self-magnetic fields inside coils could be considered as uniform. In order to admit the mutual magnetic field to be uniform too, the receiver coil is assumed to be located inside the transmitter coil (Fig. 5b).

If the transmitter coil is supplied with a time variable current i_1, a self-magnetic field will occur in the adjacent area (explained by the Ampere's law), which partially crosses the turns of the receiver coil. As a result, a voltage occurs at the terminals of the receiver coil (explained by the Faraday law), which supplies the load resistance R. The transmitter coil self-magnetic field strength is expressed using the Ampere's law for the closed curve Γ_1 which bounds the surface $S_{\Gamma 1}$ and follows the axis inside the coil and a random path outside it (Fig. 5a).
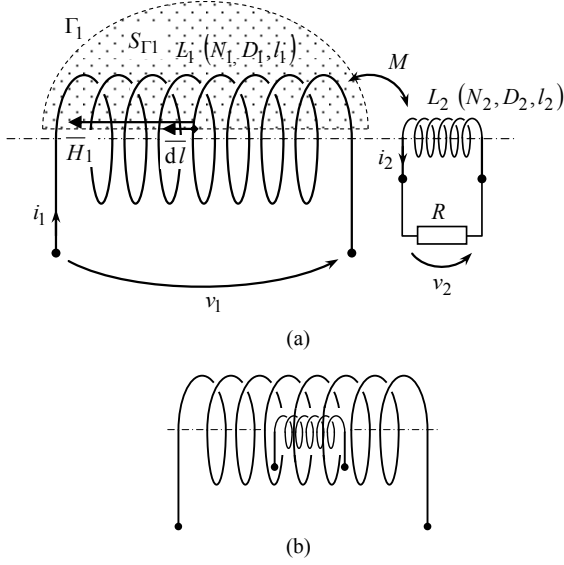
Fig. 5. Inductive coupling structure.

In the above-mentioned assumptions, by neglecting the field outside the coil, local magnetic field quantities inside the coil are calculated:

$$\int_{\Gamma_1} \overline{H}_1 \cdot \overline{\mathrm{d}l} = N_1 i_1 \text{ , from where } H_1 = \frac{N_1 i_1}{l_1},$$

$$B_1 = \frac{\mu_0 N_1 i_1}{l_1}. \qquad (13)$$

The self-magnetic flux and the self-inductance of the coil are calculated simply, as follows:

$$\Phi_1 = N_1 B_1 \cdot \frac{\pi D_1^2}{4} = \frac{\pi \mu_0 D_1^2 N_1^2 i_1}{4 l_1},$$

$$L_1 = \frac{\Phi_1}{i_1} = \frac{\pi \mu_0 D_1^2 N_1^2}{4 l_1}. \qquad (14)$$

The self-inductance of the receiver coil is expressed in a similar manner, by ignoring the presence of the transmitter coil:

$$\Phi_2 = N_2 B_2 \cdot \frac{\pi D_2^2}{4} = \frac{\pi \mu_0 D_2^2 N_2^2 i_2}{4 l_1}, \ L_2 = \frac{\pi \mu_0 D_2^2 N_2^2}{4 l_2}. \qquad (15)$$

The mutual flux, computed in the hypothesis shown in Fig. 5b, as well as the mutual inductance are:

$$\Phi_{21} = N_2 B_1 \cdot \frac{\pi D_2^2}{4} = \frac{\pi \mu_0 D_2^2 N_1 N_2 i_1}{4 l_1}, \qquad (16)$$

$$M = L_{21} = \frac{\Phi_{21}}{i_1} = \frac{\pi \mu_0 D_2^2 N_1 N_2}{4 l_1}. \qquad (17)$$

The electromotive force induced in the receiver coil, numerically equal to the voltage across its terminals in no-load conditions is computed using the Faraday's law on the closed curve Γ_2 which follows its turns and closes

between the terminals on a random path (not shown in Figure 5):

$$v_{20} = -\frac{\mathrm{d}\Phi_{21}}{\mathrm{d}t} = -\frac{\pi \mu_0 D_2^2 N_1 N_2}{4 l_1} \cdot \frac{\mathrm{d}i_1}{\mathrm{d}t} = -M \frac{\mathrm{d}i_1}{\mathrm{d}t}. \quad (18)$$

If this voltage has the same sense as v_2 shown in Fig. 5a, current   occurs when a load is present. This current generates the self-magnetic field of the receiver coil, with the magnetic flux   given by (15). By ignoring the presence of the transmitter coil, this flux leads to the voltage across the terminals:

$$v_{20}' = -\frac{\mathrm{d}\Phi_2}{\mathrm{d}t} = -\frac{\pi \mu_0 D_2^2 N_2^2}{4 l_1} \cdot \frac{\mathrm{d}i_2}{\mathrm{d}t} = -L_2 \frac{\mathrm{d}i_2}{\mathrm{d}t}, \quad (19)$$

which opposes to the sense of v_{20}. It therefore results that the actual load voltage across at the terminals of the receiver coil is:

$$v_2 = M \frac{\mathrm{d}i_1}{\mathrm{d}t} - L_2 \frac{\mathrm{d}i_2}{\mathrm{d}t}. \qquad (20)$$

The voltage across the terminals of the transmitter coil can be expressed in a similar manner:

$$v_1 = L_1 \frac{\mathrm{d}i_1}{\mathrm{d}t} - M \frac{\mathrm{d}i_2}{\mathrm{d}t}. \qquad (21)$$

In case of distorted mains, if the transmitter coil is supplied with the voltage $v_1(t) = \sqrt{2}V_1 \sin(\omega t + \gamma)$, with complex image $\underline{V}_1 = V_1 \exp(j\gamma)$, relations (20), (21) become:

$$\begin{aligned}\underline{V}_1 &= j\omega L_1 \underline{I}_1 - j\omega M \underline{I}_2 \\ \underline{V}_2 &= j\omega M \underline{I}_1 - j\omega L_2 \underline{I}_2\end{aligned}. \qquad (22)$$

Considering the obvious relation $\underline{V}_2 = R \cdot \underline{I}_2$ and by introducing the coupling factor $k = M / \sqrt{L_1 L_2}$, the coil currents and the input impedance $\underline{Z}_1 = \underline{V}_1 / \underline{I}_1$ are:

$$\underline{I}_1 = \frac{R + j\omega L_2}{\omega L_1 \left[-\omega L_2 (1 - k^2) + jR \right]} \cdot \underline{V}_1;$$

$$\underline{I}_2 = \frac{jk\sqrt{L_1 L_2}}{L_1 \left[-\omega L_2 (1 - k^2) + jR \right]} \cdot \underline{V}_1; \qquad (23)$$

$$\underline{Z}_1 = \frac{\omega^2 L_1 L_2 R k^2}{R^2 + \omega^2 L_2^2} + j\omega L_1 \cdot \left(1 - \frac{\omega^2 L_2^2 k^2}{R^2 + \omega^2 L_2^2} \right).$$

The active and reactive powers delivered by the power source are:

$$P_1 = \mathrm{Re}(\underline{Z}_1) I_1^2 = \frac{L_2 R k^2 V_1^2}{L_1 \left[R^2 + \omega^2 L_2^2 (1 - k^2)^2 \right]} = P_2;$$

$$Q_1 = \mathrm{Im}(\underline{Z}_1) I_1^2 = \frac{R^2 + \omega^2 L_2^2 (1 - k^2)}{\omega L_1 \left[R^2 + \omega^2 L_2^2 (1 - k^2)^2 \right]} \cdot V_1^2 \qquad (24)$$

The last expression denotes that the reactive power is quite high, with a minimum of $Q_{1\min} = V_1^2 / \omega L_1$ for the extreme values of the coupling factor ($k = 0$ and $k = 1$). As a result, the reactive component of the current causes important losses on the input resistance, which includes the resistance of the transmitter coil and the internal resistance of the power source, with a corresponding decrease of the power transfer efficiency. Therefore, if resonance operating conditions are accomplished both for the transmitter and for the receiver circuit, then the input reactive power is minimized and a better efficiency is obtained. We prove this scenario for a series-series resonance structure (Fig. 6a), where the two capacitors are chosen to ensure the voltage resonance at the same frequency for the transmitter and for the receiver circuit. For the numerical application:

$$L_1 = L_2 = 98.8\mu\text{H},$$
$$C_1 = C_2 = 7.91\text{nF},$$
$$R_1 = 5\Omega, R = 10\Omega$$

and coupling factor of $k = 0.1$, at the resonance frequency of $f_0 = 180.125\,\text{kHz}$, an efficiency of 72% is obtained.
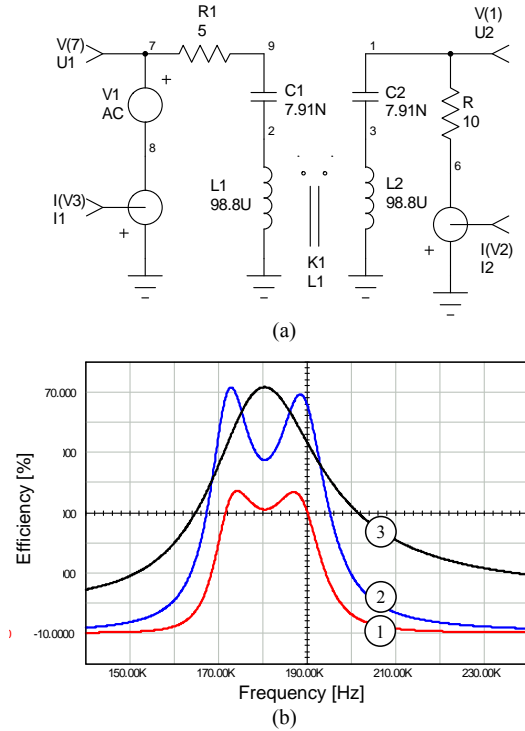

(a)

(b)

Fig. 6. Inductive power transfer system with series-series resonance:
(a) – SPICE diagram; (b) – Numerical simulation results.

The dependence of power transfer efficiency with respect to the power source frequency, obtained through a numerical SPICE simulation, is shown in Figure 6b (curve 3) next to the load power (curve 1) and the active power delivered by the source (curve 2).

Although the power transferred to load does not reach its peak value at resonance frequency, it is noticed that for its peak value, which is 15% greater, the input power becomes 40% higher, so that the power transfer efficiency is getting much worse.

IV. FIELDS OF APPLICATION AND EXPERIMENTAL RESULTS

Power transfer systems prove their utility in fields with fast development in recent years, such as battery charging systems in electric and hybrid vehicles in motion or in rest [8], battery charging systems in consumer electronics (mobile phones, computer systems, tablets and other mobile data terminals), various applications for explosive-risk environments, applications in robotics, battery charging for implanted biomedical devices, power supply for small communities with no classical power grids.

It can also be noticed that the contactless power transfer systems could be combined with data transmission systems with minimum costs. Figure 7 shows the structure of a complex system proposed by the authors for battery charging of full electric vehicles, where the power transfer is combined with data transfer required for the control of the charging process and for automatic positioning of the vehicle in front of the transmitter coil. The power transfer is achieved between the transmitter circuit (2) or fixed power station and the receiver circuit (3) or mobile power station (docked on the vehicle) separated by a gap of length (d). The transfer of power is of inductive type, as described in section III. The power transmitted to the load (5) is in the range of kW to provide charging times similar to plugin charging systems. The power static converter with auto-adaptive frequency (1) has an original design to provide the resonance working conditions for transmitter and receiver circuits and to compensate the deviations of system parameters caused by the variable load. The power converter (4) assures optimum operating conditions for charging the battery regardless of its charging state. The battery charging state and the evolution of the charging process are monitored and the information is transmitted through wireless communication (7) to the monitoring and control unit (6) which controls the power converters (1) and (4) to always obtain peak values of the transferred power at high efficiencies, with unity power factor at the power source terminals.

The design characteristics and relative position of the transmitter and receiver coils are of major importance for the energy efficiency of the whole system. Figure 8 shows some experimental models of planar type coils, manufactured with litzwire.

The experimental setup shown in Figure 9a was built to validate the results of our theoretical research and to study the influence of the relative position of coils for a wide range of working frequencies; it allows controllable deviations along all three axes. It also allows installing ferrite-based magnetic field concentrators, suitable for high frequency operation in order to improve the coupling factor (Fig. 9b) and to minimize the leakage magnetic fields according to ICNIRP guidelines [9].

The experimental tests are in progress, and their results will be disseminated at a later time.
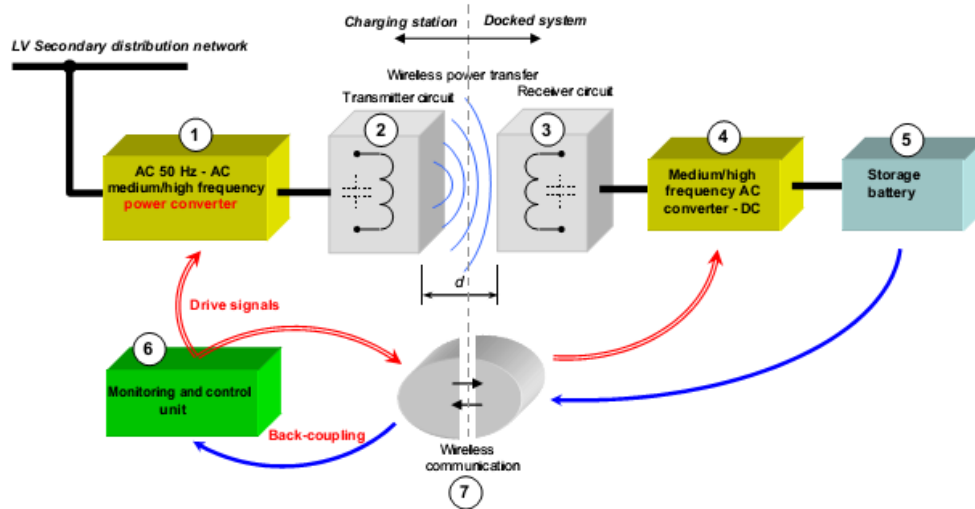
Fig. 7. Block diagram of power and data transfer system for battery charging in electric vehicles.
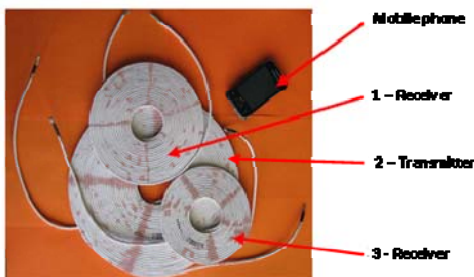

Fig. 8. Experimental models of planar coils for battery charging systems of electric vehicles. 1 – Diameter 205/60 mm; Litzwire 4.1x4.1mm, 300x0.2mm; 50 µH; 16 mΩ; 2 – Diameter 310/60 mm; Litzwire 4.1x4.1mm, 300x0.2mm; 74 µH; 36,4 mΩ; 3 – Diameter 170/60 mm; Litzwire 4.1x4.1mm, 300x0.2mm; 11 µH; 11 mΩ.
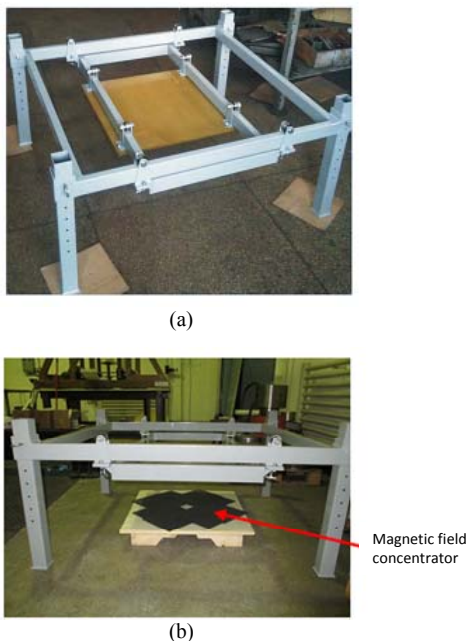

(a)

(b)

Fig. 9. Experimental setup to study of inductive coupling system performance.

V. CONCLUSIONS

The paper focuses on theoretical analysis of near field power transfer systems. It presents the principles of contactless power transfer through capacitive and respectively inductive coupling, in terms of load power and transfer efficiency. It shows the most important practical applications and focuses on inductive transfer systems for batteries charging in electric vehicles, as an application of great practical interest. Theoretical results were proven by numerical simulations, and experimental validation is in progress, using our dedicated experimental setup. The paper follows the current trends of the scientific world, as response to market demands for efficient and innovative technical solutions for contactless power transfer.

REFERENCES

[1] K. Fotopoulou, B.W. Flynn, *Wireless Power Transfer in Loosely Coupled Links: Coil Misalignment Model*, IEEE Transactions on Magnetics, Vol. 47, No. 2, February 2011.

[2]   K. Jingook, F. Bien, *Electric field coupling technique of wireless power transfer for electric vehicles*, IEEE TENCON Spring Conference, 2013, pp. 267-271.

[3]   C.C. Chan, K.T. Chau, *An Overview of Power Electronics in Electric Vehicles*, IEEE Transactions on Industrial Electronics, Vol. 44, No. 1, February 1997, pp. 3-13.

[4]   *SAE Electric Vehicle Inductive Coupling Recommended Practice*, SAE 5-1773, Feb. 1, 1995.

[5]   A.P. Sample, D.A. Meyer, J.R. Smith, *Analysis, Experimental Results, and Range Adaptation of Magnetically Coupled Resonators for Wireless Power Transfer*, IEEE Transactions on Industrial Electronics, Vol. 58, No. 2, February 2011, pp. 544-554.

[6]   J. I. Agbinya (Editor), *Wireless Power Transfer, River Publishers Series in Communications*, Denmark, 2012, ISBN: 978-87-92329-23-3.

[7]   Acute Market Reports, *Wireless Car Charging Market, Shares, Strategies and Forecasts, Worldwide, 2013 to 2019*, published on May 1, 2016. Available: http://www.acutemarketreports.com.

[8]   S. Ahn, N.P. Suh, D.H. Cho, *Charging up the Road*, IEEE Spectrum, vol. 50, no. 4, Apr. 2013, pp. 44-50.

[9]   ICNIRP (International Commission on Non-Ionizing Radiation Protection), *Guidelines for limiting exposure to time-varying electric, magnetic, and electromagnetic fields (up to 300GHz)*, Health Phys, 74(4), pp. 494-522, 1998.

[10]   D. Kishan; P.S. Rao Nayak, *Wireless power transfer technologies for electric vehicle battery charging — A state of the art*, 2016 International Conference on Signal Processing, Communication, Power and Embedded System (SCOPES), 2016, pp. 2069 - 2073.